Journal Pre-proofs

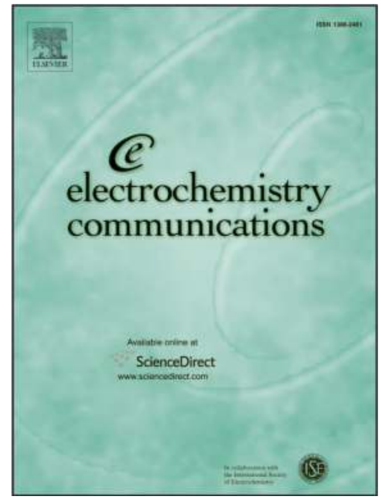

Nb-based MXenes for the efficient electrochemical sensing of small biomolecules in the anodic potential

P. Abdul Rasheed, Ravi P. Pandey, Tricia Gomez, Khadeeja A. Jabbar, Kaitlyn Prenger, Michael Naguib, Brahim Aïssa, Khaled A. Mahmoud

PII: S1388-2481(20)30162-4
DOI: https://doi.org/10.1016/j.elecom.2020.106811
Reference: ELECOM 106811

To appear in: *Electrochemistry Communications*

Received Date: 21 July 2020
Revised Date: 3 August 2020
Accepted Date: 6 August 2020

Please cite this article as: P. Abdul Rasheed, R.P. Pandey, T. Gomez, K.A. Jabbar, K. Prenger, M. Naguib, B. Aïssa, K.A. Mahmoud, Nb-based MXenes for the efficient electrochemical sensing of small biomolecules in the anodic potential, *Electrochemistry Communications* (2020), doi: https://doi.org/10.1016/j.elecom.2020.106811

Nb-based MXenes for the efficient electrochemical sensing of small biomolecules in the anodic potential

P. Abdul Rasheed[1], Ravi P. Pandey[1], Tricia Gomez[1], Khadeeja A. Jabbar[1], Kaitlyn Prenger[2], Michael Naguib[2], Brahim Aïssa[1], Khaled A. Mahmoud[1,3]*

[1]Qatar Environment and Energy Research Institute (QEERI), Hamad Bin Khalifa University (HBKU), Qatar Foundation, P.O. Box 34110, Doha, Qatar

[2]Department of Physics and Engineering Physics, Tulane University, New Orleans, LA 70118, USA

[3]Department of Physics & Mathematical Engineering, Faculty of Engineering, Port Said University, 42523 Port Said, Egypt

* Corresponding author:
E-mail: kmahmoud@hbku.edu.qa, Fax: +974 4454 41528, Phone: +974 44541694

Abstract

In this work, we study the electrochemical performance of Nb_2CT_x and $Nb_4C_3T_x$ MXenes in aqueous media and their application as a sensing platform for small biomolecules. Both Nb_2CT_x and $Nb_4C_3T_x$ are electrochemically stable up to an anodic potential of 0.5 V. It was found that $Nb_4C_3T_x$ is more electrochemically active than Nb_2CT_x. Based on this, $Nb_4C_3T_x$ was evaluated for the electrochemical detection of aqueous media solutions containing ascorbic acid, uric acid and dopamine. This work opens the door for the wider application of Nb-based MXenes in aqueous electrochemical sensing applications.

Keywords: Niobium, MXene, electrochemical stability, oxygen reduction reaction, sensors, small biomolecule detection.

1. Introduction

Two-dimensional (2D) nanomaterials have emerged as one of the most attractive sensing materials in the past decade due to their unique morphology, wide range of tunable compositions and physicochemical properties [1-3]. Recently, 2D MXenes have gained great attention due to their large group of carbides, nitrides, and carbonitrides (+30 members) and their unique properties [4-7]. The properties of MXene, such as excellent electrical conductivity and hydrophilicity [8], make them promising candidates for numerous applications such as energy storage [9-12], environmental remediation [13-18], biomedical applications [19-23], and electrochemical sensing [24-30]. $Ti_3C_2T_x$ and its related composites have been the most extensively investigated type of MXene in different electrochemical sensing applications [27, 31]. $Ti_3C_2T_x$ MXene was only stable in the cathodic potential window, however in the anodic potential it forms an irreversible anodic oxidation at ~430 mV [27]. Different nanocomposites of $Ti_3C_2T_x$ with metal nanoparticles (NPs) have been developed to overcome the instability issues in the anodic potential window [24, 32]. In such case, $Ti_3C_2T_x$ acts simultaneously as a substrate and a reducing agent (i.e. to reduce the metal salt to NPs). This partial oxidation has caused a significant reduction of the $Ti_3C_2T_x$ nanocomposite electrochemical activity as compared to bare $Ti_3C_2T_x$ [24, 32].

Nb_2CT_x and $Nb_4C_3T_x$ are members of the MXenes family, prepared by etching of the A-element from the layered ternary carbides of Nb_2AlC and Nb_4AlC_3 MAX phases, respectively [33, 34]. Recently, Nb MXenes and their composites have been successfully used in many energy applications [6, 35-38], as well as some environmental and biomedical applications including dye adsorption [39], hematopoietic recovery [33], cancer therapy [5, 19, 40], and photocatalytic hydrogen evolution [41]. The good electrochemical performance of $Nb_4C_3T_x$ MXene can be attributed to its high electronic conductivity which makes electron transport more efficient [35]. Meanwhile, the interlayer spacing of $Nb_4C_3T_x$-based electrodes enhanced by insertion and de-insertion of cations which leads to improved electrochemical performance. The intercalation capacity of cations and atoms was found to be higher in $Nb_4C_3T_x$ in comparison to Nb_2CT_x [34]. The Nb_2CT_x-PVP electrode showed large negative current density at the potential of -0.7 V in the presence of both O_2 and H_2O_2, indicating the catalytic activity of oxygen reduction reactions (ORR) and the elimination ability of H_2O_2 of Nb_2CT_x-PVP [33]. In our previous work, $Nb_4C_3T_x$-modified glassy carbon electrode was used for the electrochemical detection of Pb^{2+} ions owing to their large interlayer spacing and high electrochemical activity [42].

In this work, we investigate the electrochemical stability in the anodic potential and electrochemical behavior towards ORR of Nb-MXenes (Nb_2CT_x and $Nb_4C_3T_x$) and the sensing capability of $Nb_4C_3T_x$-modified glassy carbon electrode (GCE) towards the detection of small biomolecules such as ascorbic acid (AA), uric acid (UA), and dopamine (DA). To the best of our knowledge, this is the first report discussing the electrochemical sensing capability of $Nb_4C_3T_x$ for the detection of small biomolecules.

2. Experimental

2.1. Materials

Ascorbic acid (AA) (≥99%), dopamine hydrochloride (DA), uric acid (UA) (≥99%), NaOH, phosphate buffer (PB) solution, $K_3[Fe(CN)_6]$ (99%), and $K_4[Fe(CN)_6]\cdot 3H_2O$ (≥99%) were purchased from Sigma Aldrich, USA. Powders of niobium (99.98%, -325 mesh), aluminum (99.9%, -325 mesh), and carbon (99%, 7−11 micron) were purchased from Alfa Aesar, USA.

2.2. Synthesis and characterization of Nb_2CT_x and $Nb_4C_3T_x$

The synthesis and etching of MAX materials (Nb_2AlC and Nb_4AlC_3) were synthesized according to earlier reports [34, 36, 42]. The multilayered Nb_2CT_x and $Nb_4C_3T_x$ (ML-Nb_2CT_x and ML-$Nb_4C_3T_x$) MXenes were prepared by selective etching of Al layer using hydrofluoric acid (HF) from their MAX phases Nb_2AlC and Nb_4AlC_3, respectively, as described previously [38, 42]. The delamination of ML-Nb_2CT_x and ML-$Nb_4C_3T_x$ were carried out in degassed DI water using probe sonication (Cole Parmer, Ultrasonic Processor, 60% amplitude, 750 W) at 20 °C, under a flow of Ar for 1 h, followed by freeze-drying. The resulting solution was centrifuged at 5000 rpm for 10 minutes and decanted followed by freeze drying to get delaminated Nb_2CT_x or $Nb_4C_3T_x$ nanosheets (DL-Nb_2CT_x or DL-$Nb_4C_3T_x$). The morphology of prepared DL-Nb_2CT_x and DL-$Nb_4C_3T_x$ MXenes was studied using FEI Quanta 650 FEG scanning electron microscopy (SEM). Bruker D8 Advance (Bruker AXS, Germany) X-ray diffractometer with Cu-Kα radiation (λ = 1.54056 Å) was used to obtain wide angle X-ray diffractograms (XRD).

2.3. Electrochemical analysis

A homogenous aqueous suspension of Nb_2CT_x or $Nb_4C_3T_x$ (0.2 mg/mL) was made by sonication for 1 min. Then, 6 μL of this suspension was deposited onto the polished GCE surface and followed by drying at room temperature under Ar overnight. The modified GCE was transferred to an electrochemical work station (CHI760E potentiostat (CHI, Texas, USA)) with a conventional three electrode system. The modified GCE was used as the working electrode, Pt wire as the counter electrode and Ag/AgCl electrode as the reference electrode respectively. The electrochemical stability analysis was carried out by cyclic voltammetry (CV) in a 0.1 M PB solution (pH 7) at a potential range between -0.3 and 1 V. Cyclic voltammograms of ORR run were performed in 0.1 M NaOH under O_2 as well as N_2 atmosphere. To evaluate the sensing capability of $Nb_4C_3T_x$-modified GCE, CV experiments were carried out in a 0.1 M PB solution (pH 7) containing the desired concentration of biomolecules (DA, AA and UA) at potential ranges between -0.3 and 0.5 V. All CV analysis was performed at a scan rate of 100 mVs^{-1}. Differential pulse voltammetry (DPV) analysis was carried out in 0.1 M PB solution (pH 7) in the potential range from -0.2 to 0.5 V with an amplitude of 0.05 V with an increment of 8 mV.

3. Results and Discussion

3.1. Material characterization

Delaminated Nb-MXene nanosheets were prepared according to our previous work [42]. Although the full characterization of the material was discussed elsewhere, here we have used the SEM images to confirm the wrinkled nanosheets morphology of both DL-$Nb_4C_3T_x$ and DL-Nb_2CT_x (Fig. 1(a and b)). Energy-dispersive spectroscopy (EDS) analysis showed the presence of fluorine, oxygen, carbon and niobium elements in both MXenes (Table S1) [42]. The XRD pattern of DL-Nb_2CT_x and DL-$Nb_4C_3T_x$ and their corresponding MAX phases are given in Fig 1(c). After etching, the (002) diffraction peak of Nb_2AlC was broadened and shifted significantly toward a lower 2θ angle from 12.8° to 7.87° and the *c*-lattice parameter (*c*-LP) of DL-Nb_2CT_x was calculated from this peak as 22.44 Å [6]. Similarly, the (002) diffraction peak of Nb_4AlC_3 was shifted to 5.94° from 7.33° and the *c*-LP of DL-$Nb_4C_3T_x$ was calculated as 29.7 Å [6, 43]. This down shifting of (002) peak and the diminishing of the MAX peaks confirms the successful preparation and delamination of the DL-MXenes [6, 35, 39]. Previous studies have confirmed our observation that DL-$Nb_4C_3T_x$ usually has larger d-spacing than DL-Nb_2CT_x by ~3 Å which could be explained as the interplanar distance increases with atomic layer (*n*) in the MXenes [35, 44]. Evidently, $Nb_4C_3T_x$/GCE demonstrated higher electron transfer kinetics than Nb_2CT_x/GCE [42]. The higher conductivity of $Nb_4C_3T_x$ than Nb_2CT_x can be explained by the higher '*n*' value of $Nb_4C_3T_x$ (n=3) than Nb_2CT_x (n=1), since $Nb_4C_3T_x$ has more MAX character due to the additional NbC layers [45]. In addition, larger interlayer spacing of $Nb_4C_3T_x$ allows faster adsorption and intercalation of ions, which enhances ion diffusion and charge transport of the electrolyte towards enhancement in the electrochemical activity [43].

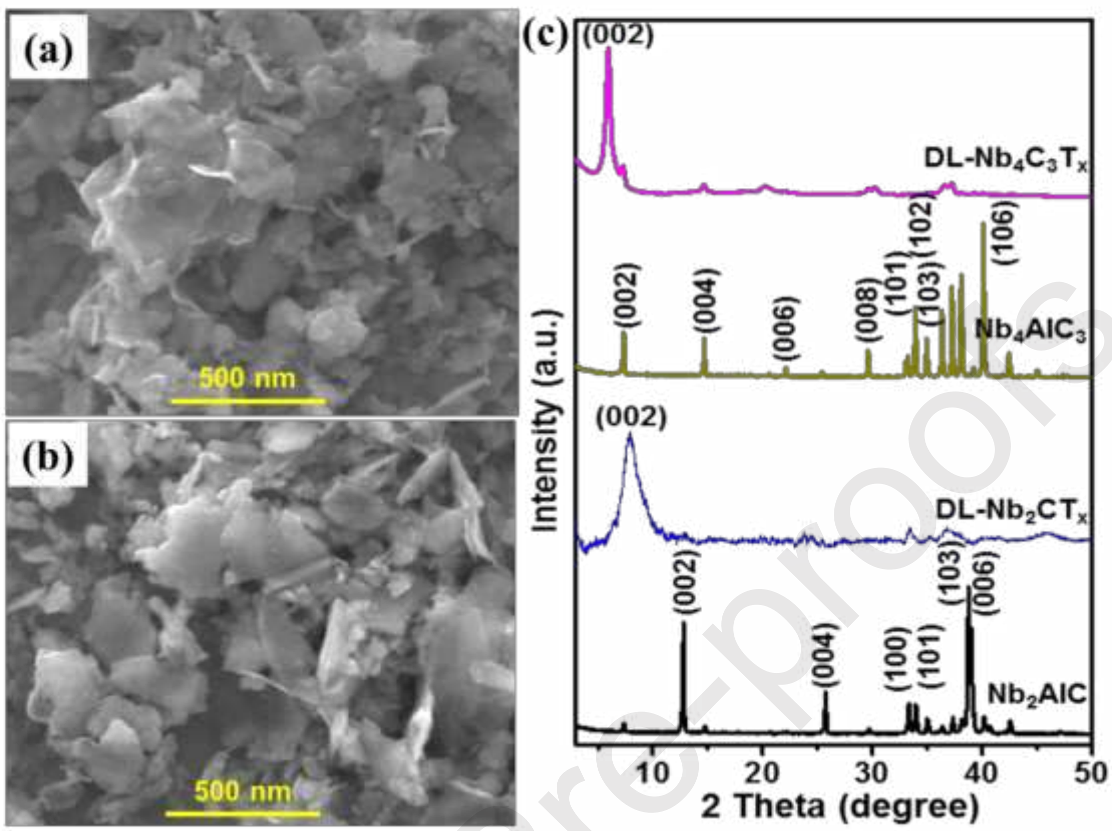

Fig. 1. SEM image of (a) DL-Nb_2CT_x and (b) DL-$Nb_4C_3T_x$. (c) XRD pattern of Nb_2AlC, Nb_4AlC_3, DL-Nb_2CT_x and DL-$Nb_4C_3T_x$.

3.2. Electrochemical characterization of Nb_2CT_x and $Nb_4C_3T_x$

Here, we have used cyclic voltammetry (CV) to investigate in more detail the electrochemical behavior of the Nb MXenes in the anodic potential window. As shown in Fig. 2(a), the CV obtained in 0.1 M PB solution from 0 to 1.0 V showed an anodic oxidation for both Nb_2CT_x/GCE and $Nb_4C_3T_x$/GCE with an onset potential of around +0.5 V. However, the peak current is higher for $Nb_4C_3T_x$/GCE. The higher oxidation current for $Nb_4C_3T_x$ can be attributed to its higher electron transfer kinetics than Nb_2CT_x [42, 46]. The difference between the first scan and fifth scan for $Nb_4C_3T_x$/GCE is around 2.4 μA at a potential of 1 V as seen in the inset of Fig. 2(a). This shows that the partial oxidation of $Nb_4C_3T_x$ occurs during the anodic scan above +0.5 V. Similarly,

Nb_2CT_x/GCE also showed the same oxidation behavior but with less peak intensity than $Nb_4C_3T_x$. The difference between the first scan and fifth scan for Nb_2CT_x/GCE is around 2 μA at a potential of 1 V (Fig. S1). This oxidation behavior of both Nb MXenes is entirely different from $Ti_3C_2T_x$, where irreversible oxidation of $Ti_3C_2T_x$ occurred upon exposure to an anodic potential around 0.43 V [27]. Since the oxidation onset potential for both Nb MXenes starts at +0.5 V, another cyclic voltammogram was run below the onset potential +0.5 V to evaluate the stability below the onset potential. Fig 2(b) shows the cyclic voltammograms of Nb MXenes/GCE in 0.1 M PB buffer (pH 7) in the potential window from -0.3 V to 0.5 V. The peak current difference between the first and second scan is only around 0.1 μA and the difference reaches only up to 0.15 μA for the fifth scan. Similar electrochemical behavior is observed for Nb_2CT_x with a peak current difference of 0.2 μA between the first and fifth scans (Fig. S1). This negligible current difference after multiple scans shows that both Nb MXenes are electrochemically stable up to a potential of 0.5 V.

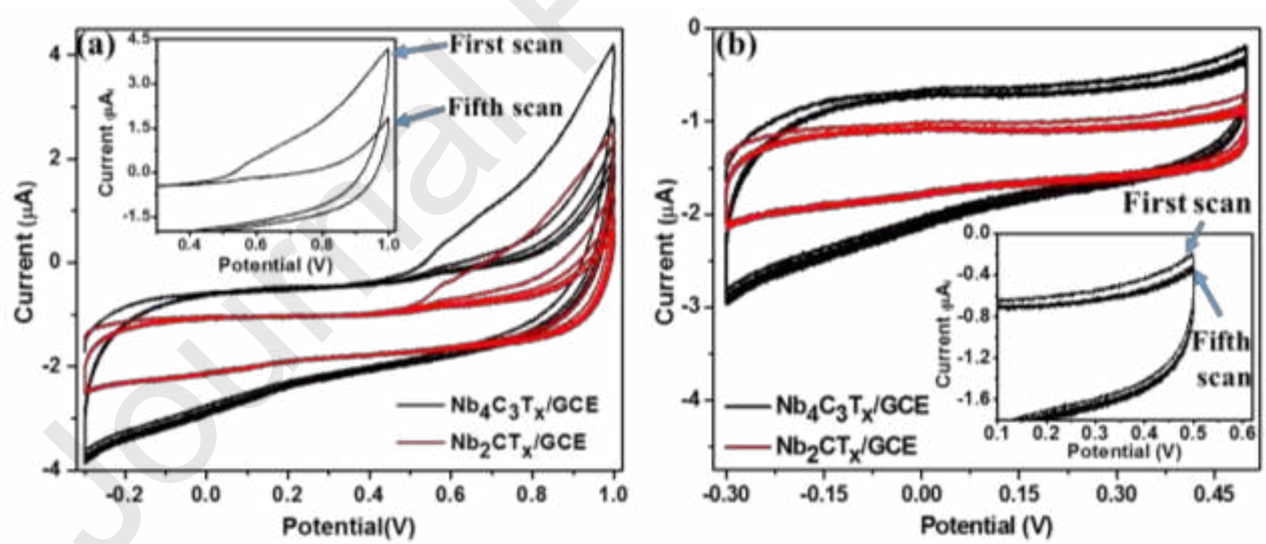

Fig. 2. (a) Cyclic voltammograms of Nb_2CT_x/GCE and $Nb_4C_3T_x$/GCE in 0.1 M PB buffer (pH 7) in the potential window from -0.3 V to 1.0 V. Inset is the magnified version for $Nb_4C_3T_x$/GCE showing the difference between the first and fifth scan. (b) Cyclic voltammograms of Nb_2CT_x/GCE and $Nb_4C_3T_x$/GCE in 0.1 M PB buffer (pH 7) in the potential window from -0.3 V to 0.5 V. Inset is the magnified version for $Nb_4C_3T_x$/GCE showing the difference between the first and fifth scan.

The oxygen reduction reaction (ORR) is an essential reaction in biological processes and in energy-converting systems. Developing high performance alternative electrocatalytic systems for ORR remains a significant challenge. Different studies showed that $Ti_3C_2T_x$ MXenes can be a good substrate for accommodation of various types of nanomaterials for effective ORR reactions considering their excellent conductivity and hydrophilic surfaces for easy modification with prominent stability [47-49]. Here, the electrocatalytic ORR activities of Nb MXenes/GCE were evaluated in N_2/O_2 saturated alkaline media of NaOH (0.1 M) and compared with $Ti_3C_2T_x$. For bare GCE, featureless voltammetric currents were observed in the potential range of -1.0 V to 0 V in both O_2 or N_2 saturated solutions indicating that there are no active redox species in the electrolyte (Fig. S2). As shown in Fig. 3, a definite reduction peak occurs at around -0.45 V for both Nb MXenes/GCE in the O_2 saturated solution, while there is no specific peak in the N_2 saturated solution, indicating that O_2 is reduced on both electrodes. In addition, the change in current density for $Nb_4C_3T_x$/GCE is significantly higher than Nb_2CT_x/GCE that in GCE, indicating high oxygen reduction activity for $Nb_4C_3T_x$ [50]. The oxygen reduction current of $Nb_4C_3T_x$/GCE was calculated to be 120 $\mu A.cm^{-2}$ and the corresponding current for Nb_2CT_x/GCE was 90 $\mu A.cm^{-2}$, both values are significantly higher than bare GCE (42 $\mu A.cm^{-2}$) at -0.45V. The previous studies found that the oxygen reduction current of $Ti_3C_2T_x$ (63 $\mu A.cm^{-2}$ at −0.55 V) and oxidized $Ti_3C_2T_x$ (80 $\mu A.cm^{-2}$ at −0.55 V) are low even at a lower reduction potential compared to both Nb MXenes [27]. From these results, it is found that pristine $Nb_4C_3T_x$ and Nb_2CT_x were not highly efficient for catalyzing the ORR similar to pristine $Ti_3C_2T_x$. However, it is expected that $Nb_4C_3T_x$-based heterostructures could be a more efficient ORR catalyst than $Ti_3C_2T_x$ considering their higher electrochemical activity and larger interlayer spacing which may enhance the interfacial interactions and charge separation towards ORR.

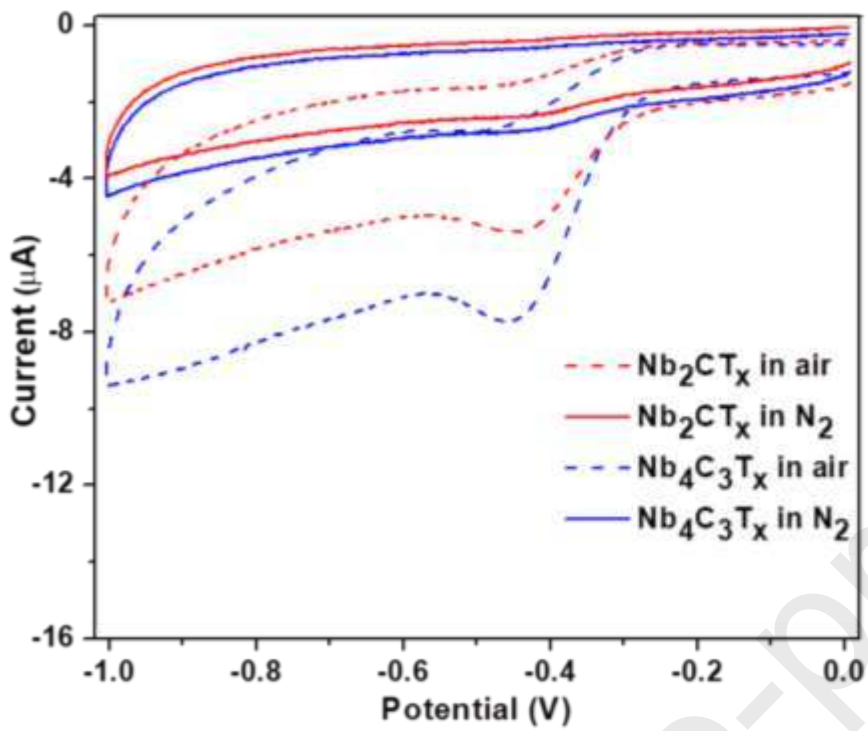

Fig. 3. Cyclic voltammograms of ORR run on Nb_2CT_x/GCE and $Nb_4C_3T_x$/GCE in 0.1 M NaOH under air and N_2 atmosphere at a scan rate 100 mVs^{-1}.

3.3. Electrochemical response of $Nb_4C_3T_x$/GCE to small biomolecules

The electrocatalytic responses of the $Nb_4C_3T_x$/GCE have been tested for sensing of small biomolecules such as AA, DA and UA. DA and UA are biomolecules widely distributed in the human body with important roles in many physiological processes, and AA is an essential nutrient for the human body, usually coexisting with DA and UA in extracellular fluid [51]. $Nb_4C_3T_x$ has the highest electrochemical activity up to 0.5 V, which is suitable with the electrochemical peak of these biomolecules. The CV responses for $Nb_4C_3T_x$/GCE in the presence of different biomolecules (10 μM of DA, AA and UA) in 0.1 M PB solution is shown in Fig. 4(a). An enhanced response is observed for $Nb_4C_3T_x$/GCE compared to bare GCE, confirming the electrochemical activity of $Nb_4C_3T_x$. In addition, oxidation peaks are visible for biomolecules at different potentials (~0.15 V for DA, ~0.27 V for AA and ~0.35 V for UA). To find the accurate oxidation potential for different biomolecules, DPV was run and the results confirmed the oxidation potential for DA, AA and UA at 0.14 V, 0.26 V and 0.35 V respectively (Fig. 4(b)). From the CV and DPV analysis, it is confirmed that the sensitive detection of DA, AA and UA is possible with $Nb_4C_3T_x$-modified GCE.

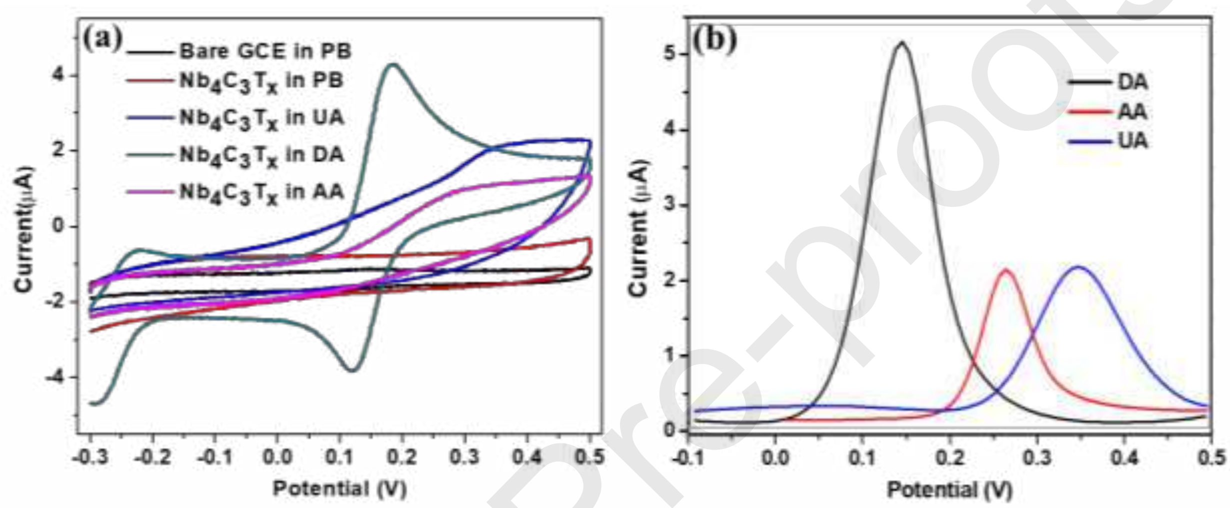

Fig. 4. (a) CV responses for $Nb_4C_3T_x$/GCE in the presence of 10 μM AA, UA and DA in 0.1 M PB solution (pH 7). (b) Differential pulse voltammetry shows the respective peak positions for AA, UA and DA.

The quantitative detection of DA was further performed by DPV and amperometry analysis using $Nb_4C_3T_x$/GCE. As shown in Fig. 5(a), the DPV peak current increases with increasing DA concentrations from 0 to 10 μM. Two different linear ranges are observed in the calibration plot; one from 50 nM to 1 μM and another from 1 μM to 10 μM (Fig. 5(b)). The limit of detection was calculated using the 3σ method [52] from the linear range 50 nM to 1 μM as 29 nM. In addition, amperometric measurements at +0.14 V were performed after the sequential addition of DA into 0.1 M PB (pH 7) at time intervals of 40 s. As shown in Fig. 5(c), the first measurable response was observed after the addition of 50 nM DA and then the current response increased with an increase in the DA concentrations. From the amperometric responses, the plot of ΔI as a function of the concentration of DA was made and the limit of detection was calculated from this plot as 23 nM using the 3σ method (Fig. 5(d)) [52]. The limit of detection of the $Nb_4C_3T_x$-based DA sensor is comparable with $Ti_3C_2T_x$-based electrochemical sensors for DA detection [53-55]. Field effect transistors based on ultrathin conductive $Ti_3C_2T_x$-MXene micropatterns were already employed for the detection of DA with a detection limit of 100 nM [55]. $Ti_3C_2T_x$-based nanocomposite ($Ti_3C_2T_x$/DNA/Pd/Pt) showed the detection limit of 30 nM [53], while the Nafion stabilized $Ti_3C_2T_x$-based DA sensor showed a lower detection limit of 3 nM [54]. In our case, a detection limit of 23 nM was achieved by using only bare $Nb_4C_3T_x$, which can be further enhanced by surface modification and nano-composition.

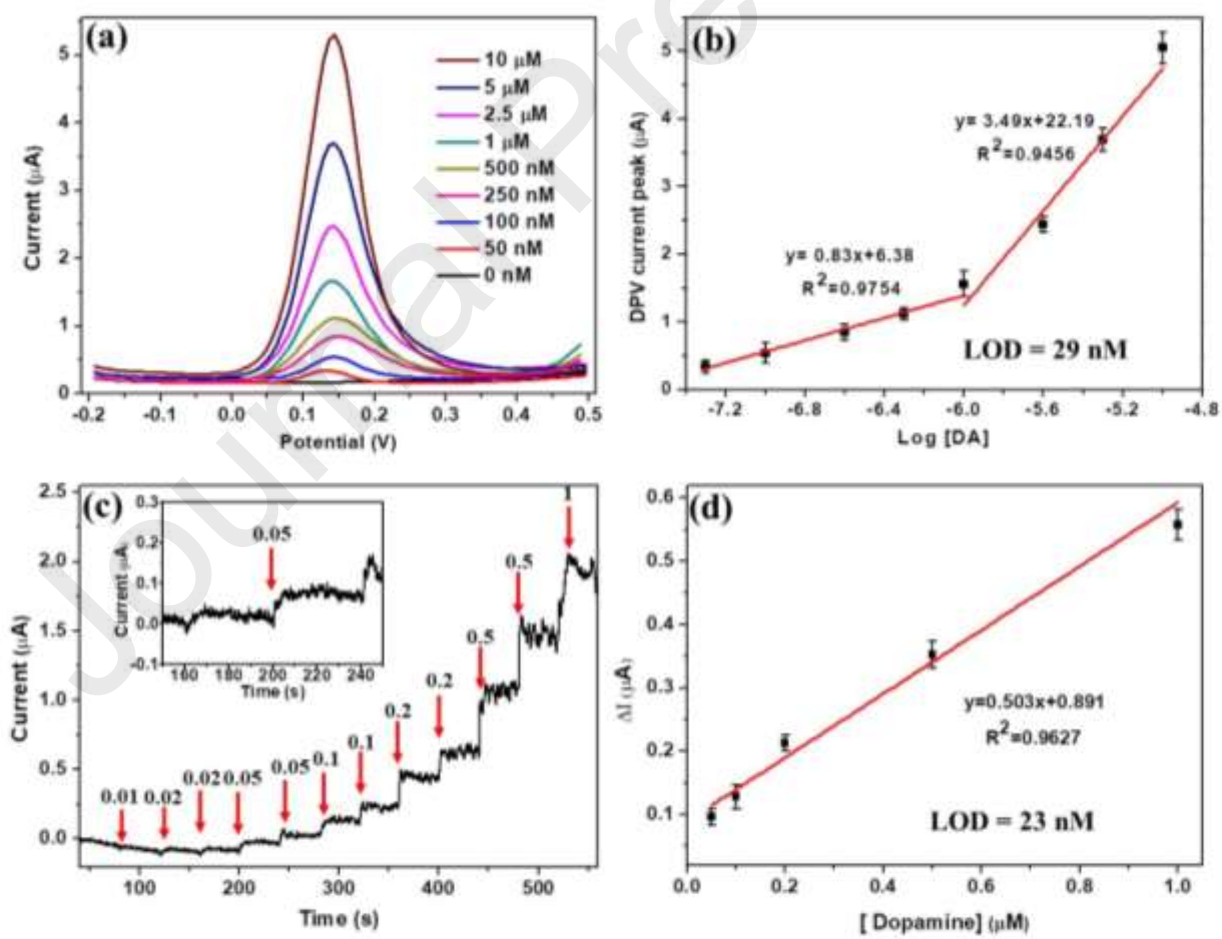

Fig. 5. (a) The DPV of the $Nb_4C_3T_x$/GCE in 0.1 M PB solution with different concentrations of DA. (b) The plot between the DPV peak current vs log DA concentrations. (c) Amperometric (*I*–*t*) curve of the $Nb_4C_3T_x$/GCE with successive additions of DA from 10 nM to 1 µM in 0.1 M PB (pH 7), at +1.4 V. (d) The calibration plot of Δ*I* vs concentration of DA from the *I*–*t* curve. Error bars show the standard deviation for three repetitive measurements.

The selectivity analysis of the $Nb_4C_3T_x$/GCE shows only ~2% change in the peak current of DA in the presence of interfering agents like AA and UA (Fig. 6). However, there is a small shift in the peak position of DA in the presence of AA and UA and it is clearly distinguishable from the individual peaks of AA and UA. In addition, the DPV current response of DA changes to only 5% in the presence of interfering agents with 100 times concentration of DA (Fig. 6). The repeatability analysis of the sensor with four identical $Nb_4C_3T_x$/GCE electrodes in the presence of 1 µM DA show good repeatability between multiple electrodes with an RSD value of 1.27 (Fig. S3). The stability analysis of the $Nb_4C_3T_x$/GCE shows 97.1% of the initial current value with RSD of 2.38 after keeping the electrode at 4°C for one week. Hence, it is confirmed that the developed sensor is highly stable, repeatable, and sensitive, and it can be used for sensitive DA detection in the presence of interfering agents.

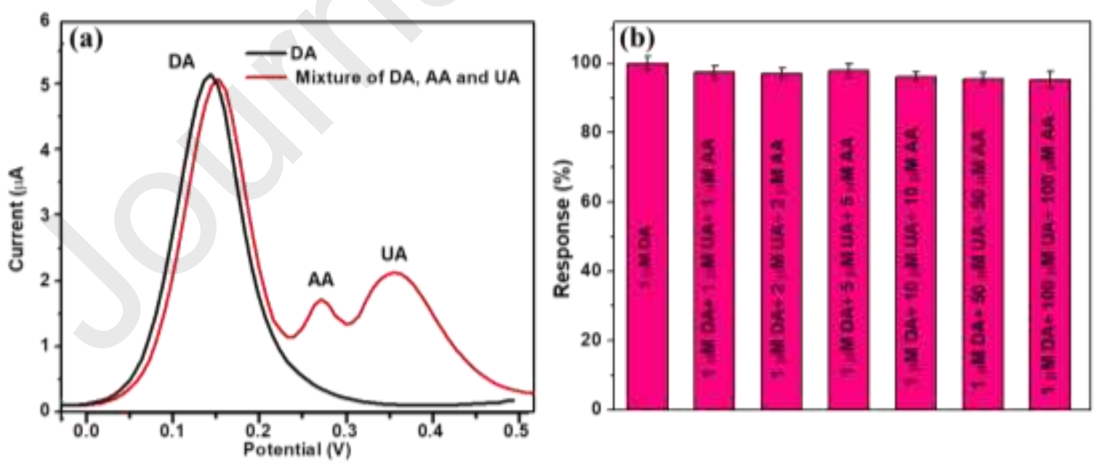

Fig. 6. (a) DPV response of the $Nb_4C_3T_x$/GCE in the presence of 1 μM DA, and mixture of DA, AA and UA. (b) The DPV response of $Nb_4C_3T_x$/GCE with 1 μM DA in comparison with 1 μM DA along with different concentrations of 1−100 μM of AA and UA.

4. Conclusions

The electrochemical behavior of Nb_2CT_x and $Nb_4C_3T_x$ was investigated in detail to explore their potential in electrochemical sensing applications. It was found that both Nb_2CT_x and $Nb_4C_3T_x$ can be used in the anodic potential window up to 0.5 V. The pristine $Nb_4C_3T_x$ and Nb_2CT_x might not be the best candidate for catalyzing the ORR; however, heterostructures of $Nb_4C_3T_x$ and Nb_2CT_x can improve their catalytic activity for ORR. The detailed electrochemical analysis showed that $Nb_4C_3T_x$ can be used as an immobilization platform for sensitive detection of DA with a wide linear range and detection limit of 23 nM. This work demonstrates the high potential of $Nb_4C_3T_x$ towards the development of different electrochemical sensors.

Acknowledgement

The authors acknowledge the financial support of Qatar National Research Fund (A member of Qatar Foundation) through the NPRP grant NPRP9-254-2-120. The authors acknowledge A. R Shetty, and M. Pasha of QEERI Core Labs for XRD and SEM measurements, respectively.

Appendix A. Supplementary data

Supplementary data to this article can be found online at ***.

References

[1] Y. Chen, C. Tan, H. Zhang, L. Wang, Two-dimensional graphene analogues for biomedical applications, Chemical Society Reviews, 44 (2015) 2681-2701.
[2] K. Yang, L. Feng, X. Shi, Z. Liu, Nano-graphene in biomedicine: theranostic applications, Chemical Society Reviews, 42 (2013) 530-547.
[3] Y. Chen, L. Wang, J. Shi, Two-dimensional non-carbonaceous materials-enabled efficient photothermal cancer therapy, Nano Today, 11 (2016) 292-308.

[4] M. Naguib, V.N. Mochalin, M.W. Barsoum, Y. Gogotsi, 25th anniversary article: MXenes: A new family of two-dimensional materials, Advanced Materials, 26 (2014) 992-1005.
[5] H. Lin, S. Gao, C. Dai, Y. Chen, J. Shi, A two-dimensional biodegradable niobium carbide (MXene) for photothermal tumor eradication in NIR-I and NIR-II biowindows, Journal of the American Chemical Society, 139 (2017) 16235-16247.
[6] O. Mashtalir, M.R. Lukatskaya, M.-Q. Zhao, M.W. Barsoum, Y. Gogotsi, Amine-assisted delamination of Nb2C MXene for Li-ion energy storage devices, Advanced Materials, 27 (2015) 3501-3506.
[7] K. Rasool, R.P. Pandey, P.A. Rasheed, S. Buczek, Y. Gogotsi, K.A. Mahmoud, Water treatment and environmental remediation applications of two-dimensional metal carbides (MXenes), Materials Today, (2019).
[8] M. Naguib, O. Mashtalir, J. Carle, V. Presser, J. Lu, L. Hultman, Y. Gogotsi, M.W. Barsoum, Two-dimensional transition metal carbides, ACS Nano, 6 (2012) 1322-1331.
[9] M.R. Lukatskaya, O. Mashtalir, C.E. Ren, Y. Dall'Agnese, P. Rozier, P.L. Taberna, M. Naguib, P. Simon, M.W. Barsoum, Y. Gogotsi, Cation intercalation and high volumetric capacitance of two-dimensional titanium carbide, Science, 341 (2013) 1502-1505.
[10] M. Naguib, J. Come, B. Dyatkin, V. Presser, P.-L. Taberna, P. Simon, M.W. Barsoum, Y. Gogotsi, MXene: a promising transition metal carbide anode for lithium-ion batteries, Electrochemistry Communications, 16 (2012) 61-64.
[11] D. Sun, M. Wang, Z. Li, G. Fan, L.-Z. Fan, A. Zhou, Two-dimensional Ti_3C_2 as anode material for Li-ion batteries, Electrochemistry Communications, 47 (2014) 80-83.
[12] Y. Xie, Y. Dall'Agnese, M. Naguib, Y. Gogotsi, M.W. Barsoum, H.L. Zhuang, P.R.C. Kent, Prediction and characterization of MXene nanosheet anodes for non-lithium-ion batteries, ACS Nano, 8 (2014) 9606-9615.
[13] G. Zou, J. Guo, Q. Peng, A. Zhou, Q. Zhang, B. Liu, Synthesis of urchin-like rutile titania carbon nanocomposites by iron-facilitated phase transformation of MXene for environmental remediation, Journal of Materials Chemistry A, 4 (2016) 489-499.
[14] V.M. Hong Ng, H. Huang, K. Zhou, P.S. Lee, W. Que, J.Z. Xu, L.B. Kong, Recent progress in layered transition metal carbides and/or nitrides (MXenes) and their composites: synthesis and applications, Journal of Materials Chemistry A, 5 (2017) 3039-3068.
[15] Q. Zhang, J. Teng, G. Zou, Q. Peng, Q. Du, T. Jiao, J. Xiang, Efficient phosphate sequestration for water purification by unique sandwich-like MXene/magnetic iron oxide nanocomposites, Nanoscale, 8 (2016) 7085-7093.
[16] A. Shahzad, K. Rasool, W. Miran, M. Nawaz, J. Jang, K.A. Mahmoud, D.S. Lee, Two-dimensional Ti_3C_2Tx MXene nanosheets for efficient copper removal from water, ACS Sustainable Chemistry & Engineering, 5 (2017) 11481-11488.
[17] Y. Ying, Y. Liu, X. Wang, Y. Mao, W. Cao, P. Hu, X. Peng, Two-dimensional titanium carbide for efficiently reductive removal of highly toxic chromium(VI) from water, ACS Applied Materials & Interfaces, 7 (2015) 1795-1803.
[18] K. Rasool, R.P. Pandey, P.A. Rasheed, G.R. Berdiyorov, K.A. Mahmoud, MXenes for environmental and water treatment applications, in: 2D Metal Carbides and Nitrides (MXenes), Springer, 2019, pp. 417-444.
[19] X. Han, X. Jing, D. Yang, H. Lin, Z. Wang, H. Ran, P. Li, Y. Chen, Therapeutic mesopore construction on 2D Nb_2C MXenes for targeted and enhanced chemo-photothermal cancer therapy in NIR-II biowindow, Theranostics, 8 (2018) 4491-4508.
[20] K. Huang, Z. Li, J. Lin, G. Han, P. Huang, Two-dimensional transition metal carbides and nitrides (MXenes) for biomedical applications, Chemical Society Reviews, 47 (2018) 5109-5124.
[21] H. Lin, Y. Wang, S. Gao, Y. Chen, J. Shi, Theranostic 2D tantalum carbide (MXene), Advanced Materials, 30 (2018) 1703284.

[22] Z. Liu, H. Lin, M. Zhao, C. Dai, S. Zhang, W. Peng, Y. Chen, 2D superparamagnetic tantalum carbide composite MXenes for efficient breast-cancer theranostics, Theranostics, 8 (2018) 1648-1664.
[23] C. Liu, L. Geng, Y. Yu, Y. Zhang, B. Zhao, S. Zhang, Q. Zhao, Reduction of bacterial adhesion on Ag-TiO_2 coatings, Materials Letters, 218 (2018) 334-336.
[24] P.A. Rasheed, R.P. Pandey, K.A. Jabbar, J. Ponraj, K.A. Mahmoud, Sensitive electrochemical detection of L-cysteine based on a highly stable Pd@$Ti_3C_2T_x$ (MXene) nanocomposite modified glassy carbon electrode, Analytical Methods, 11 (2019) 3851-3856.
[25] P.A. Rasheed, R.P. Pandey, K. Rasool, K.A. Mahmoud, Ultra-sensitive electrocatalytic detection of bromate in drinking water based on Nafion/ $Ti_3C_2T_x$ (MXene) modified glassy carbon electrode, Sensors and Actuators B: Chemical, 265 (2018) 652-659.
[26] H. Liu, C. Duan, C. Yang, W. Shen, F. Wang, Z. Zhu, A novel nitrite biosensor based on the direct electrochemistry of hemoglobin immobilized on MXene- Ti_3C_2, Sensors and Actuators B: Chemical, 218 (2015) 60-66.
[27] L. Lorencova, T. Bertok, E. Dosekova, A. Holazova, D. Paprckova, A. Vikartovska, V. Sasinkova, J. Filip, P. Kasak, M. Jerigova, D. Velic, K.A. Mahmoud, J. Tkac, Electrochemical performance of Ti_3C_2Tx MXene in aqueous media: towards ultrasensitive H_2O_2 sensing, Electrochimica Acta, 235 (2017) 471-479.
[28] R.B. Rakhi, P. Nayak, C. Xia, H.N. Alshareef, Novel amperometric glucose biosensor based on MXene nanocomposite, Scientific Reports, 6 (2016) 36422.
[29] F. Wang, C. Yang, M. Duan, Y. Tang, J. Zhu, TiO2 nanoparticle modified organ-like Ti_3C_2MXene nanocomposite encapsulating hemoglobin for a mediator-free biosensor with excellent performances, Biosensors and Bioelectronics, 74 (2015) 1022-1028.
[30] E.S. Muckley, M. Naguib, H.-W. Wang, L. Vlcek, N.C. Osti, R.L. Sacci, X. Sang, R.R. Unocic, Y. Xie, M. Tyagi, E. Mamontov, K.L. Page, P.R.C. Kent, J. Nanda, I.N. Ivanov, Multimodality of structural, electrical, and gravimetric responses of intercalated MXenes to water, ACS Nano, 11 (2017) 11118-11126.
[31] A. Sinha, Dhanjai, H. Zhao, Y. Huang, X. Lu, J. Chen, R. Jain, MXene: An emerging material for sensing and biosensing, TrAC Trends in Analytical Chemistry, 105 (2018) 424-435.
[32] L. Lorencova, T. Bertok, J. Filip, M. Jerigova, D. Velic, P. Kasak, K.A. Mahmoud, J. Tkac, Highly stable $Ti_3C_2T_x$ (MXene)/Pt nanoparticles-modified glassy carbon electrode for H_2O_2 and small molecules sensing applications, Sensors and Actuators B: Chemical, 263 (2018) 360-368.
[33] X. Ren, M. Huo, M. Wang, H. Lin, X. Zhang, J. Yin, Y. Chen, H. Chen, Highly catalytic niobium carbide (MXene) promotes hematopoietic recovery after radiation by free radical scavenging, ACS Nano, 13 (2019) 6438-6454.
[34] J. Yang, M. Naguib, M. Ghidiu, L.-M. Pan, J. Gu, J. Nanda, J. Halim, Y. Gogotsi, M.W. Barsoum, Two-dimensional Nb-based M_4C_3 solid solutions (MXenes), Journal of the American Ceramic Society, 99 (2016) 660-666.
[35] S. Zhao, X. Meng, K. Zhu, F. Du, G. Chen, Y. Wei, Y. Gogotsi, Y. Gao, Li-ion uptake and increase in interlayer spacing of Nb_4C_3 MXene, Energy Storage Materials, 8 (2017) 42-48.
[36] M. Naguib, J. Halim, J. Lu, K.M. Cook, L. Hultman, Y. Gogotsi, M.W. Barsoum, New two-dimensional niobium and vanadium carbides as promising materials for Li-ion batteries, Journal of the American Chemical Society, 135 (2013) 15966-15969.
[37] C. Zhang, M. Beidaghi, M. Naguib, M.R. Lukatskaya, M.-Q. Zhao, B. Dyatkin, K.M. Cook, S.J. Kim, B. Eng, X. Xiao, D. Long, W. Qiao, B. Dunn, Y. Gogotsi, Synthesis and charge storage properties of hierarchical niobium pentoxide/carbon/niobium carbide (MXene) hybrid materials, Chemistry of Materials, 28 (2016) 3937-3943.
[38] J. Zhao, J. Wen, L. Bai, J. Xiao, R. Zheng, X. Shan, L. Li, H. Gao, X. Zhang, One-step synthesis of few-layer niobium carbide MXene as a promising anode material for high-rate lithium ion batteries, Dalton Transactions, 48 (2019) 14433-14439.

[39] C. Peng, P. Wei, X. Chen, Y. Zhang, F. Zhu, Y. Cao, H. Wang, H. Yu, F. Peng, A hydrothermal etching route to synthesis of 2D MXene (Ti_3C_2, Nb_2C): Enhanced exfoliation and improved adsorption performance, Ceramics International, 44 (2018) 18886-18893.
[40] A. Jastrzebska, A. Szuplewska, A. Rozmysłowska-Wojciechowska, J. Mitrzak, T. Wojciechowski, M. Chudy, D. Moszczyńska, A. Wójcik, K. Prenger, M. Naguib, Juggling surface charges of 2D niobium carbide MXenes for a reactive oxygen species scavenging and effective targeting of the malignant melanoma cell cycle into programmed cell death, ACS Sustainable Chemistry & Engineering, 8 (2020) 7942-7951.
[41] T. Su, R. Peng, Z.D. Hood, M. Naguib, I.N. Ivanov, J.K. Keum, Z. Qin, Z. Guo, Z. Wu, One-step synthesis of Nb_2O_5/C/Nb_2C (MXene) composites and their use as photocatalysts for hydrogen evolution, ChemSusChem, 11 (2018) 688-699.
[42] P.A. Rasheed, R.P. Pandey, T. Gomez, M. Naguib, K.A. Mahmoud, Large interlayer spacing $Nb_4C_3T_x$ (MXene) promotes the ultrasensitive electrochemical detection of Pb^{2+} on glassy carbon electrodes, RSC Advances, 10 (2020) 24697-24704.
[43] S. Zhao, C. Chen, X. Zhao, X. Chu, F. Du, G. Chen, Y. Gogotsi, Y. Gao, Y. Dall'Agnese, Flexible $Nb_4C_3T_x$ film with large interlayer spacing for high-performance supercapacitors, Advanced Functional Materials, 2020, 2000815.
[44] J. Pang, R.G. Mendes, A. Bachmatiuk, L. Zhao, H.Q. Ta, T. Gemming, H. Liu, Z. Liu, M.H. Rummeli, Applications of 2D MXenes in energy conversion and storage systems, Chemical Society Reviews, 48 (2019) 72-133.
[45] M. Ghidiu, M. Naguib, C. Shi, O. Mashtalir, L.M. Pan, B. Zhang, J. Yang, Y. Gogotsi, S.J.L. Billinge, M.W. Barsoum, Synthesis and characterization of two-dimensional Nb_4C_3 (MXene), Chemical Communications, 50 (2014) 9517-9520.
[46] P. Nayak, Q. Jiang, R. Mohanraman, D. Anjum, M.N. Hedhili, H.N. Alshareef, Inherent electrochemistry and charge transfer properties of few-layered two-dimensional $Ti_3C_2T_x$ MXene, Nanoscale, 10 (2018) 17030-17037.
[47] X. Yu, W. Yin, T. Wang, Y. Zhang, Decorating g-C_3N_4 nanosheets with Ti_3C_2 MXene nanoparticles for efficient oxygen reduction reaction, Langmuir, 35 (2019) 2909-2916.
[48] Q. Xue, Z. Pei, Y. Huang, M. Zhu, Z. Tang, H. Li, Y. Huang, N. Li, H. Zhang, C. Zhi, Mn_3O_4 nanoparticles on layer-structured Ti_3C_2 MXene towards the oxygen reduction reaction and zinc–air batteries, Journal of Materials Chemistry A, 5 (2017) 20818-20823.
[49] L. Jiang, J. Duan, J. Zhu, S. Chen, M. Antonietti, Iron-cluster-directed synthesis of 2D/2D Fe–N–C/MXene superlattice-like heterostructure with enhanced oxygen reduction electrocatalysis, ACS Nano, 14 (2020) 2436-2444.
[50] I.-Y. Jeon, D. Yu, S.-Y. Bae, H.-J. Choi, D.W. Chang, L. Dai, J.-B. Baek, Formation of large-area nitrogen-doped graphene film prepared from simple solution casting of edge-selectively functionalized graphite and its electrocatalytic activity, Chemistry of Materials, 23 (2011) 3987-3992.
[51] J. Feng, Q. Li, J. Cai, T. Yang, J. Chen, X. Hou, Electrochemical detection mechanism of dopamine and uric acid on titanium nitride-reduced graphene oxide composite with and without ascorbic acid, Sensors and Actuators B: Chemical, 298 (2019) 126872.
[52] P.A. Rasheed, T. Radhakrishnan, P.K. Shihabudeen, N. Sandhyarani, Reduced graphene oxide-yttria nanocomposite modified electrode for enhancing the sensitivity of electrochemical genosensor, Biosensors and Bioelectronics, 83 (2016) 361-367.
[53] J. Zheng, B. Wang, A. Ding, B. Weng, J. Chen, Synthesis of MXene/DNA/Pd/Pt nanocomposite for sensitive detection of dopamine, Journal of Electroanalytical Chemistry, 816 (2018) 189-194.
[54] F. Shahzad, A. Iqbal, S.A. Zaidi, S.-W. Hwang, C.M. Koo, Nafion-stabilized two-dimensional transition metal carbide ($Ti_3C_2T_x$ MXene) as a high-performance electrochemical sensor for neurotransmitter, Journal of Industrial and Engineering Chemistry, 79 (2019) 338-344.

[55] B. Xu, M. Zhu, W. Zhang, X. Zhen, Z. Pei, Q. Xue, C. Zhi, P. Shi, Ultrathin MXene-micropattern-based field-effect transistor for probing neural activity, Advanced Materials, 28 (2016) 3333-3339.

Highlights

- The electrochemical performance of Nb_2CT_x and $Nb_4C_3T_x$ MXenes in aqueous media was evaluated.
- Both Nb_2CT_x and $Nb_4C_3T_x$ are electrochemically stable up to an anodic potential of 0.5 V.
- It was found that $Nb_4C_3T_x$ is more electrochemically active than Nb_2CT_x.
- $Nb_4C_3T_x$ can be used as an immobilization platform for the sensitive detection of dopamine with a detection limit of 23 nM.

Graphical Abstract

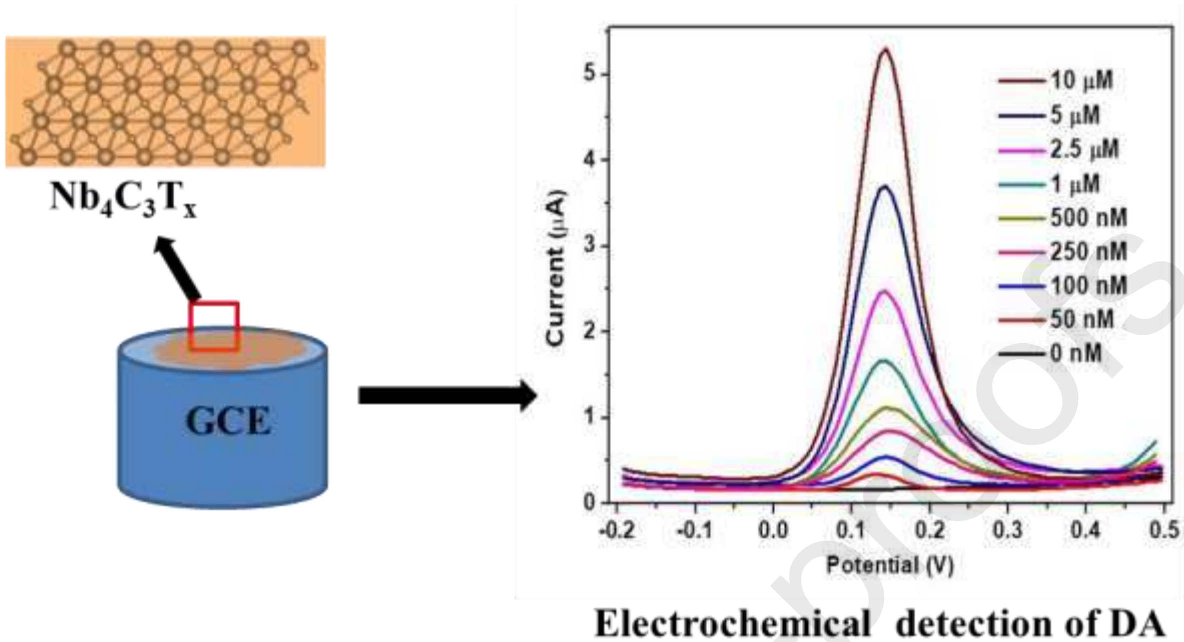

Credit author statement

Conceptualization: PAR, RPP

Data curation: PAR, KAM, MN

Formal analysis: PAR, RPP, KAM

Funding acquisition: KAM

Investigation: PAR, KAJ, TG

Methodology: PAR, RPP, TG, KP

Project administration: KAM

Supervision: KAM, MN

Validation: PAR, RPP, BA, KAM

Roles/Writing - original draft: PAR, KAJ, TG

Writing - review & editing: KP, MN, BA, KAM